

Supporting Information

Dioxygen Activation and O-O Bond Formation Reactions by Manganese Corroles

Mian Guo,[†] Yong-Min Lee,[†] Ranjana Gupta,[†] Mi Sook Seo,[†] Takehiro Ohta,[‡]
Hua-Hua Wang,[§] Hai-Yang Liu,[§] Sunder N. Dhuri,^{†,#} Ritimukta Sarangi,^{&,*} Shunichi
Fukuzumi,^{†,*} and Wonwoo Nam^{†,¶,*}

[†] *Department of Chemistry and Nano Science, Ewha Womans University, Seoul 03760, Korea*

[‡] *Picobiology Institute, Graduate School of Life Science, University of Hyogo, RSC-UH LP
Center, Hyogo 679-5148, Japan*

[§] *Department of Chemistry, South China University of Technology, Guangzhou 510641,
China*

[#] *Department of Chemistry, Goa University, Goa 403 206, India*

[&] *Stanford Synchrotron Radiation Lightsource, SLAC National Accelerator Laboratory,
Menlo Park, CA 94025, USA*

[¶] *State Key Laboratory for Oxo Synthesis and Selective Oxidation, Lanzhou Institute of
Chemical Physics, Chinese Academy of Sciences, Lanzhou 730000, China*

* E-mail: wwnam@ewha.ac.kr, fukuzumi@chem.eng.osaka-u.ac.jp,
ritis@slac.stanford.edu

Table of Contents

Table S1	S3
Figure S1	S4
Figure S2	S5
Figure S3	S6
Figure S4	S7
Figure S5	S8
Figure S6	S9
Figure S7	S10
Figure S8	S11
Figure S9	S12
Figure S10	S13
Figure S11	S14
Figure S12	S15
Figure S13	S16
Figure S14	S17
Figure S15	S18
Figure S16	S19
Figure S17	S20
Figure S18	S21
Figure S19	S22
Figure S20	S23
Figure S21	S24
Figure S22	S25
Figure S23	S26
References	S27

Table S1. EXAFS Least Squares Fitting Results

complex	coordination/path	$R(\text{\AA})^a$	$\sigma^2(\text{\AA}^2)^b$	E_0 (eV)	F^c
[(TPFC)Mn ^{III}]	4 Mn-N	1.91	470		
	6 Mn-C	2.89	863		
	12 Mn-C-N	3.15	114	-2.76	0.09
	4 Mn-C-N	3.66	938		
	8 Mn-C	4.23	575		
	8 Mn-C-N	4.78	617		
2	2 Mn-O	1.83	411		
	4 Mn-N	1.96	329		
	6 Mn-C	2.88	752	-1.43	0.15
	16 Mn-C-N	3.15	312		
	8 Mn-C-N	4.11	575		
	8 Mn-C	4.67	1208		

^aThe estimated standard deviations for the distances are in the order of $\pm 0.02 \text{ \AA}$. ^bThe σ^2 values are multiplied by 10^5 . ^cError is given by $\Sigma[(\chi_{\text{obsd}} - \chi_{\text{calcd}})^2 k^6] / \Sigma[(\chi_{\text{obsd}})^2 k^6]$. The S_0^2 factor was set at 1.

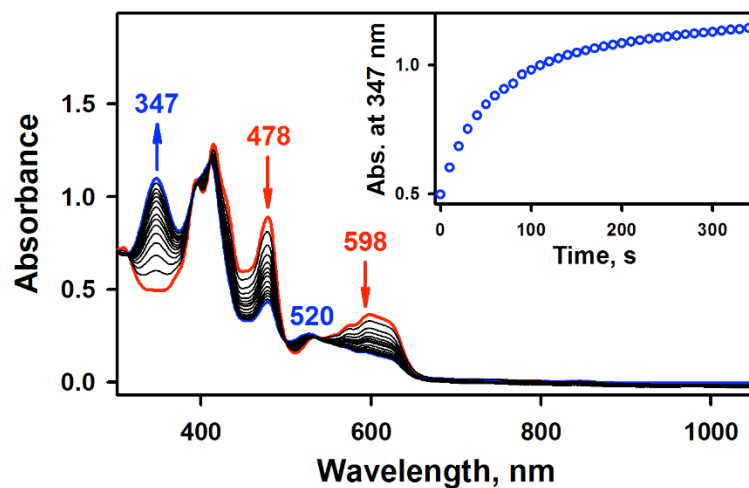


Figure S1. UV-vis spectral changes observed for the formation of **1** (blue line) in the O₂-activation by [(TPFC)Mn^{III}] (0.030 mM, red line) in the presence of TMAH (0.030 mM) under an air atmosphere in THF at 25 °C. Inset shows the time trace monitored at 347 nm due to the formation of **1**.

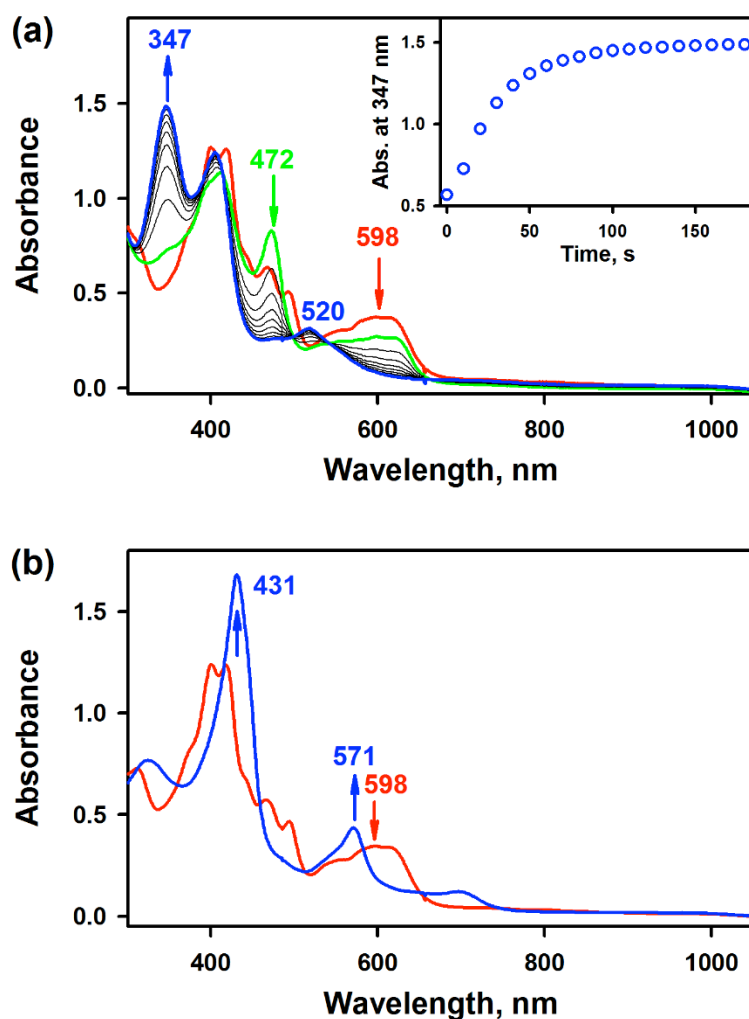


Figure S2. (a) UV-vis spectral changes observed in the reaction of $[(\text{TPFC})\text{Mn}^{\text{III}}]$ (red line; 0.030 mM) and 1-(*tert*-butylsulfonyl)-2-iodosylbenzene ($^s\text{PhIO}$, 0.060 mM) to form $[(\text{TPFC})\text{Mn}^{\text{V}}(\text{O})]$ species (**1**; blue line) through the intermediacy of green line spectrum in CH_3CN at 0 °C. Inset shows the time course monitored at 347 nm due to the formation of **1**. (b) UV-vis spectral changes observed in the reaction of $[(\text{TPFC})\text{Mn}^{\text{III}}]$ (red line; 0.030 mM) and H_2O_2 (0.12 mM) in the presence of tetramethylammonium hydroxide (TMAH; 0.60 mM) to form $[(\text{TPFC})\text{Mn}^{\text{IV}}(\text{O}_2)]^-$ species (**2**; blue line) immediately in CH_3CN at 0 °C.

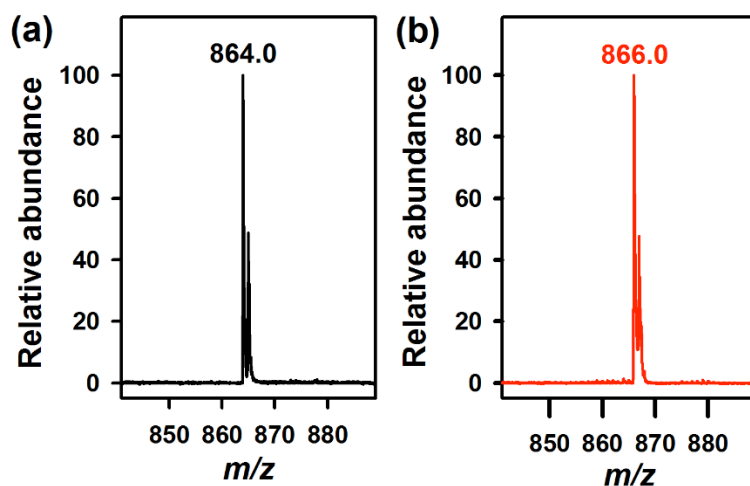


Figure S3. CSI-MS spectra of (a) $1\text{-}^{16}\text{O}$ and (b) $1\text{-}^{18}\text{O}$ recorded in positive mode. The peaks at $m/z = 864.0$ and 866.0 together with their isotope distribution patterns correspond to $[(\text{TPFC})\text{Mn}(^{16}\text{O})]$ (calcd. $m/z = 864.0$) and $[(\text{TPFC})\text{Mn}(^{18}\text{O})]$ (calcd. $m/z = 866.0$), respectively.

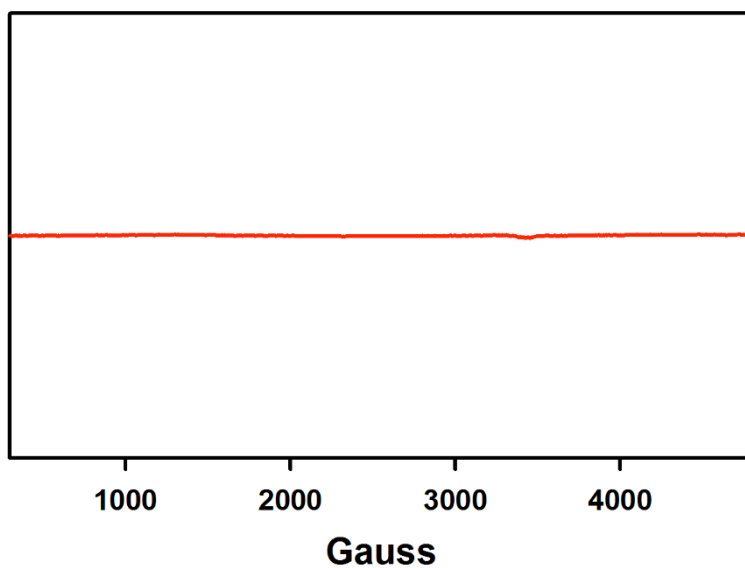


Figure S4. X-band CW-EPR spectrum of **1** produced in the O₂-activation reaction by [(TPFC)Mn^{III}] (0.10 mM) with O₂ in the presence of TMAH (0.20 mM) in tetrahydrofuran (THF) at 25 °C. Spectrum was recorded at 5 K.

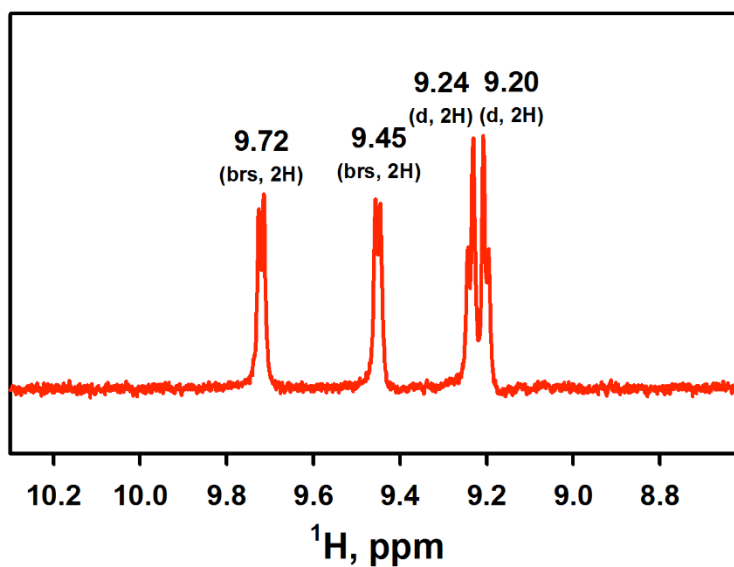


Figure S5. ¹H NMR spectrum of **1** in CD₃CN at -10 °C. Chemical shifts ($\delta = 9.72$, 9.45, 9.24 and 9.20 ppm) are quite similar to the reported values ($\delta = 9.6$, 9.3, 9.12 and 9.06 ppm) of **1** in CD₂Cl₂ at -80 °C.^{S1}

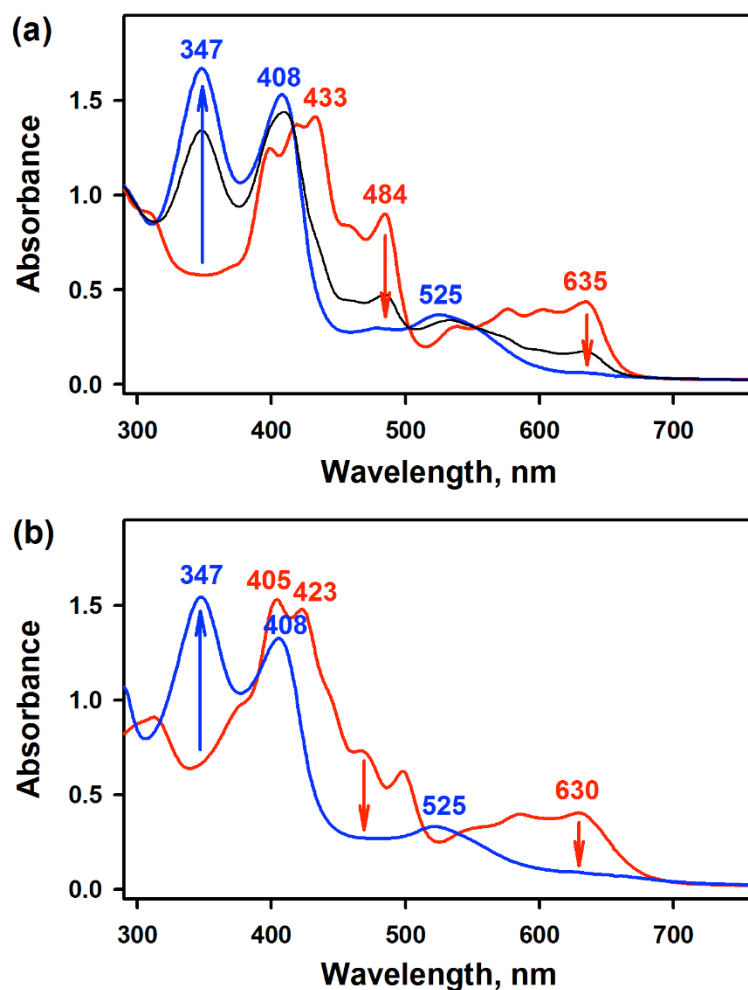


Figure S6. (a) UV-vis spectral changes showing the formation of [(TPFcCN)Mn^V(O)] (blue line) in the O₂-activation reaction by [(TPFcCN)Mn^{III}] (0.030 mM; red line) with O₂ in the presence of TMAH (0.060 mM) under an air atmosphere in THF at 25 °C. (b) UV-vis spectral changes showing the immediate formation of [(TPFcCN)Mn^{IV}(O)] (blue line) in the reaction of [(TPFcCN)Mn^{III}] (0.030 mM; red line) and ^sPhIO (0.060 mM) in CH₃CN at 0 °C.

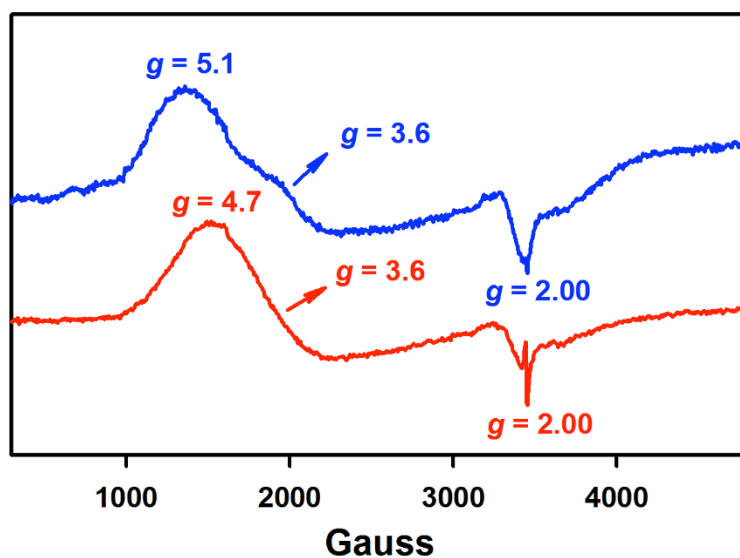


Figure S7. X-band CW-EPR spectra of $[(\text{TPFC})\text{Mn}^{\text{IV}}(\text{O}_2)]^-$ (**2**; blue line) and $[(\text{TPFcCN})\text{Mn}^{\text{IV}}(\text{O}_2)]^-$ (red line) generated in the O_2 -activation reaction by $[(\text{TPFC})\text{Mn}^{\text{III}}]$ (0.50 mM) and $[(\text{TPFcCN})\text{Mn}^{\text{III}}]$ (0.50 mM), respectively, with O_2 in the presence of TMAH (10 mM) under an air atmosphere in THF at 25 °C. Spectra were recorded at 5 K.

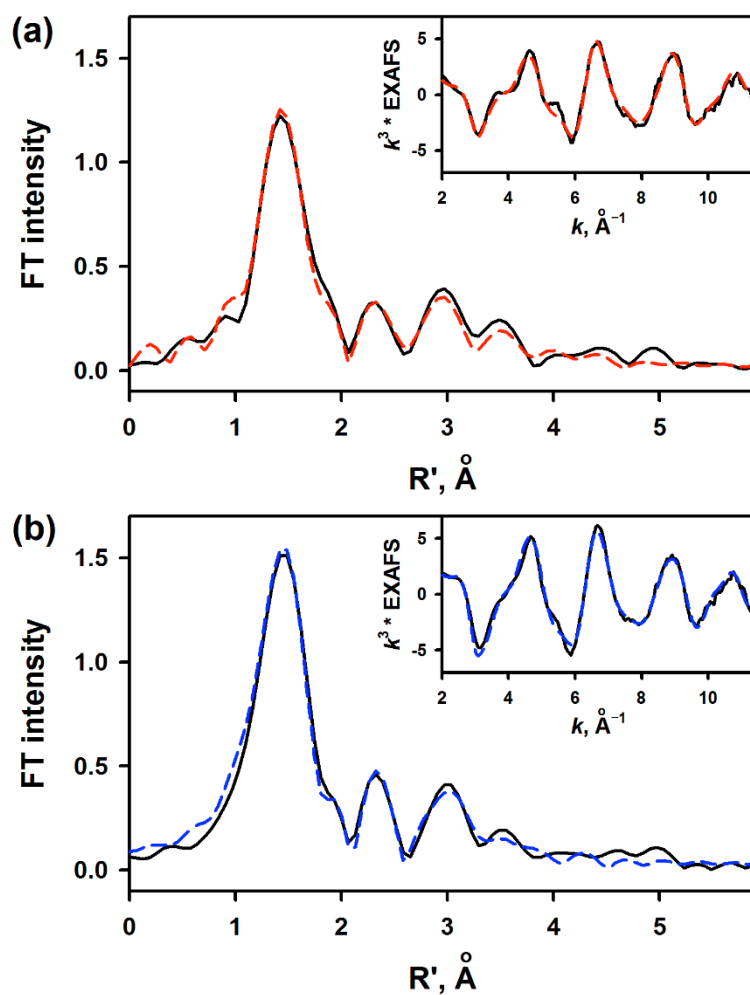


Figure S8. (a) FEFF best-fits to the Fourier Transform and EXAFS data (inset) for [Mn^{III}(TPFC)]: experimental data (black solid line) and fit (red dashed line). (b) FEFF best-fits to the Fourier Transform and EXAFS data (inset) for **2**: experimental data (black solid line) and fit (blue dashed line).

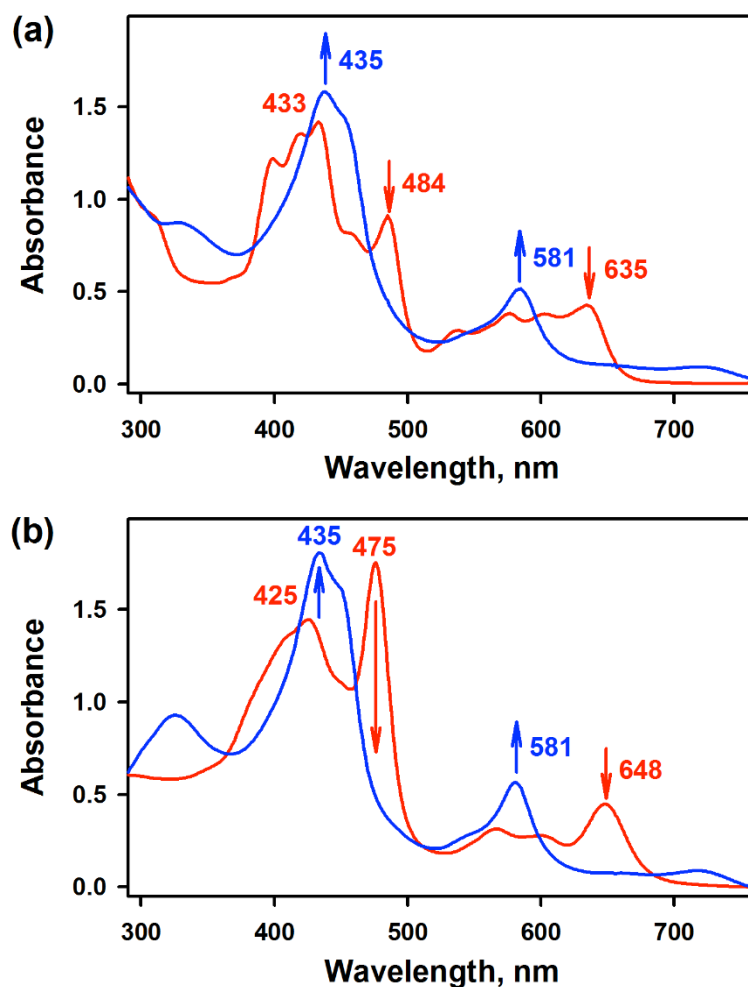


Figure S9. (a) UV-vis spectral changes observed in the O_2 -activation reaction by $[(\text{TPFcCN})\text{Mn}^{\text{III}}]$ (0.030 mM; red line) with O_2 in the presence of TMAH (0.60 mM) to form $[(\text{TPFcCN})\text{Mn}^{\text{IV}}(\text{O}_2)]^-$ (blue line) immediately under an air atmosphere in THF at 25 °C. (b) UV-vis spectral changes observed in the reaction of $[(\text{TPFcCN})\text{Mn}^{\text{III}}(\text{OH})]^-$ (0.030 mM; red line), which was produced by adding TMAH (0.60 mM) to a CH_3CN solution of $[(\text{TPFcCN})\text{Mn}^{\text{III}}]$ (0.030 mM) and H_2O_2 (0.12 mM) to form $[(\text{TPFcCN})\text{Mn}^{\text{IV}}(\text{O}_2)]^-$ (blue line) immediately at 0 °C.

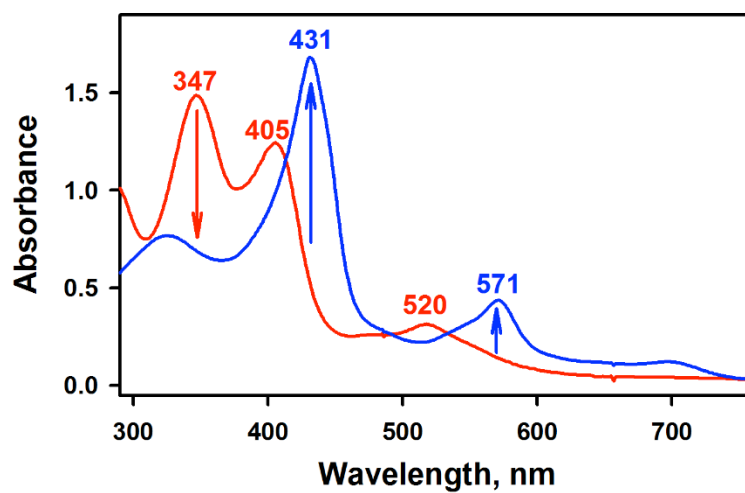


Figure S10. UV-vis spectral changes observed in the conversion of **1** (0.030 mM, red line) to **2** (blue line) upon addition of TMAH (0.60 mM) to a CH₃CN solution of **1** at 0 °C.

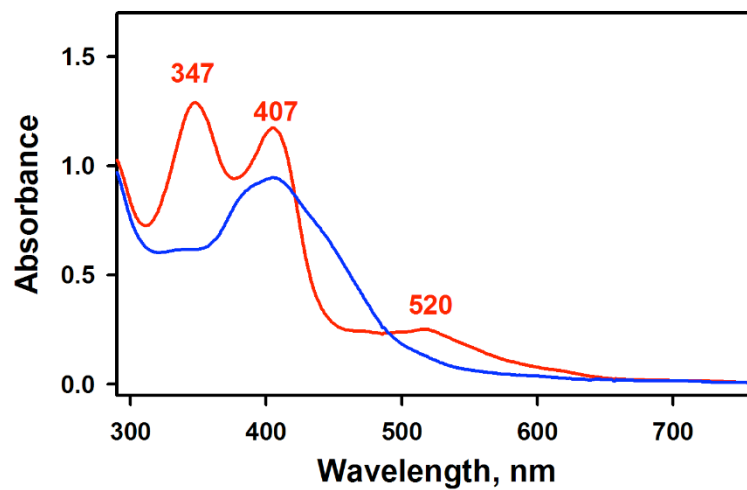


Figure S11. UV-vis spectral changes observed upon addition of HClO₄ (0.060 mM) to a CH₃CN solution **1** (red line; 0.030 mM) at 0°C, corresponding to the immediate formation of the decomposed product.^{S2}

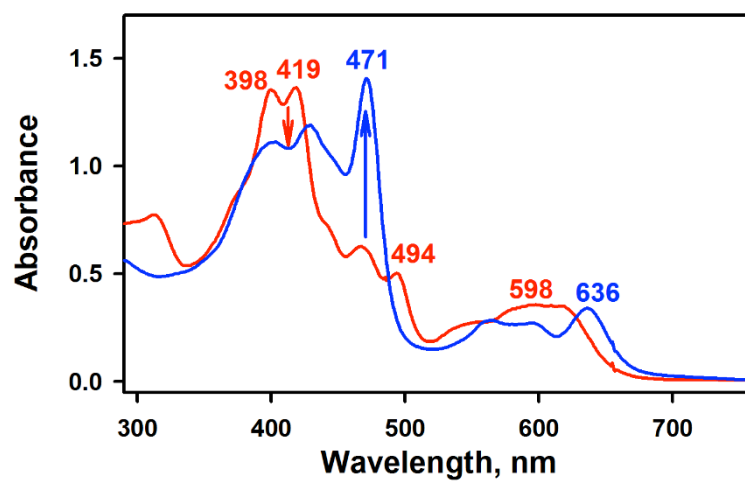


Figure S12. UV-vis spectral change observed for the formation of **3** (blue line) upon addition of TMAH (0.60 mM) to a CH₃CN solution of [(TPFC)Mn^{III}] (0.030 mM, red line) at 25 °C.

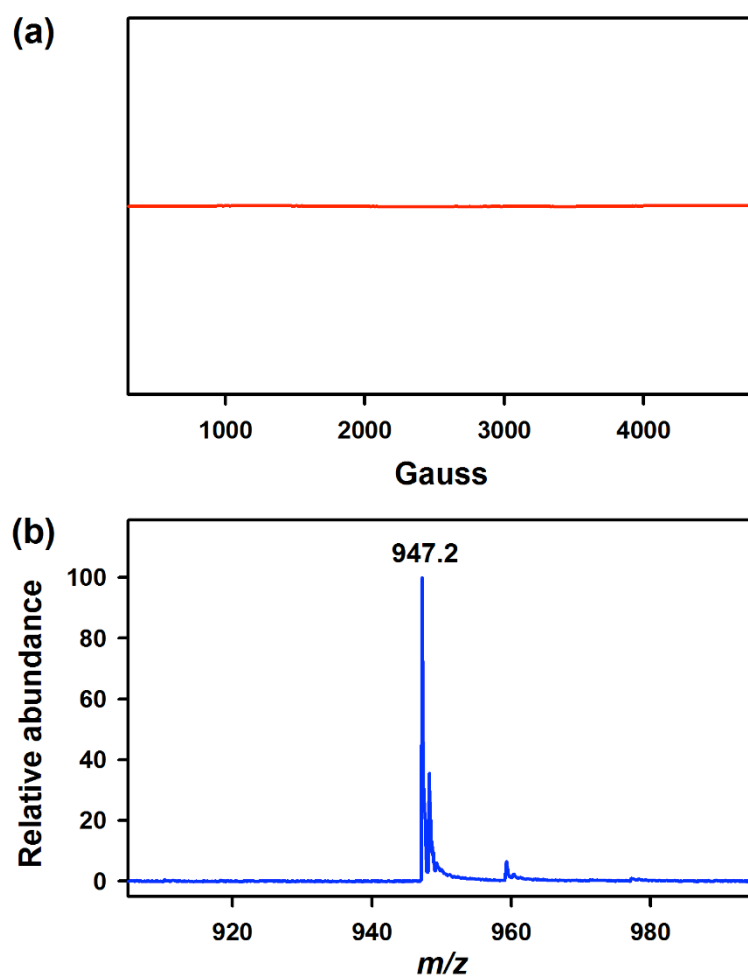


Figure S13. (a) X-band EPR spectrum of $[(\text{TPFC})\text{Mn}^{\text{III}}(\text{OH})]^-$ (**3**) produced by adding TMAH (10 mM) to a CH_3CN solution of $[(\text{TPFC})\text{Mn}^{\text{III}}]$ (0.50 mM) at 0 °C. Spectrum was recorded at 5 K. (b) CSI-MS spectrum of **3** (0.030 mM) recorded in negative mode in CH_3CN . The peak at $m/z = 947.2$ corresponds to $[(\text{TPFC})\text{Mn}^{\text{III}}(\text{OH})(\text{CH}_3\text{CN})_2]^-$ (calcd. $m/z = 947.0$).

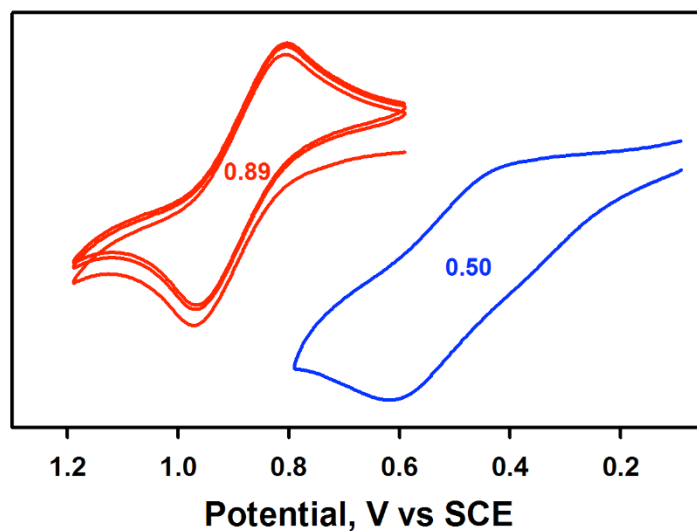


Figure S14. Cyclic voltammograms of [(TPFC)Mn^{III}] (2.0 mM) in the absence (red line) and presence (blue line) of TMAH (4.0 mM) under an Ar atmosphere in THF at 25 °C. The one-electron oxidation potential of [(TPFC)Mn^{III}] (2.0 mM) exhibited a significant negative shift from 0.89 V vs SCE in the absence of TMAH to 0.50 V vs SCE in the presence of TMAH (4.0 mM). This negative shift may result from the binding of OH⁻ to the one-electron oxidized [(TPFC)Mn^{IV}]⁺ species, which is much more acidic than [(TPFC)Mn^{III}].

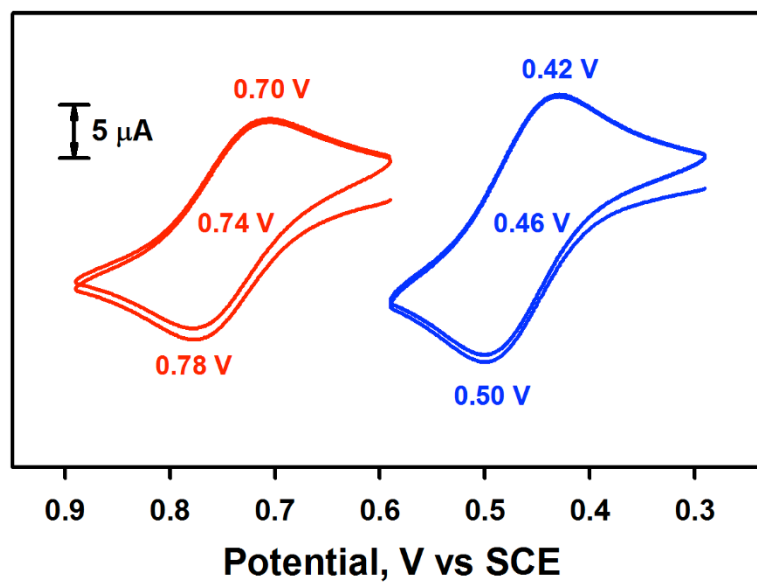


Figure S15. Cyclic voltammograms of [(TPFC)Mn^{III}] (2.0 mM) in the absence (red line) and presence (blue line) of tetrabutylammonium chloride (TMACl, 2.0 mM) in CH₃CN at 25 °C.

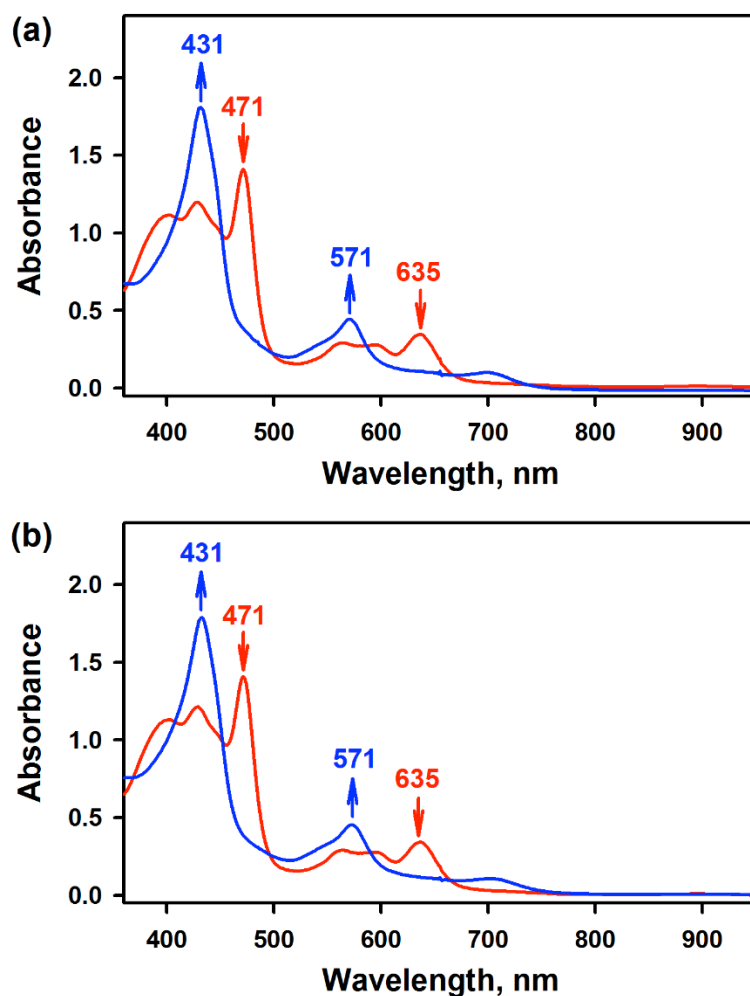


Figure S16. (a) UV-vis spectral changes observed in the immediate formation of **2** (blue line) upon addition of THF (0.12 M) to a CH₃CN solution of [(TPFC)Mn^{III}(OH)]⁻ (**3**) (0.030 mM, red line), which was produced by adding TMAH (0.60 mM) to a CH₃CN solution of [(TPFC)Mn^{III}] (0.030 mM), under an air atmosphere at 25 °C. (b) UV-vis spectral changes observed in the immediate formation of **2** (blue line) upon addition of cyclohexene (0.20 M) to a CH₃CN solution of [(TPFC)Mn^{III}(OH)]⁻ (**3**) (0.030 mM, red line), which was produced by adding TMAH (0.60 mM) to a CH₃CN solution of [(TPFC)Mn^{III}] (0.030 mM), under an air atmosphere at 25 °C.

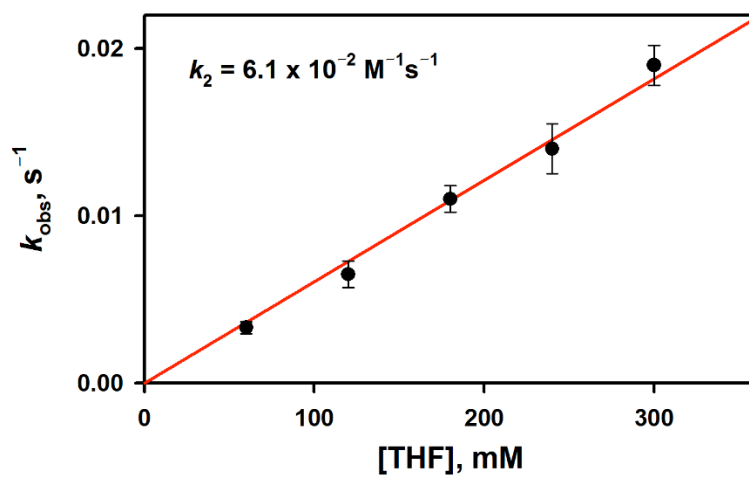


Figure S17. Plot of k_{obs} against THF concentration for the formation of **2** in the O_2 -activation by $[(\text{TPFC})\text{Mn}^{\text{III}}]$ (0.030 mM) with O_2 in the presence of TMAH (0.60 mM) under an air atmosphere in CH_3CN at $-20\text{ }^\circ\text{C}$ to determine the second-order rate constant, k_2 .

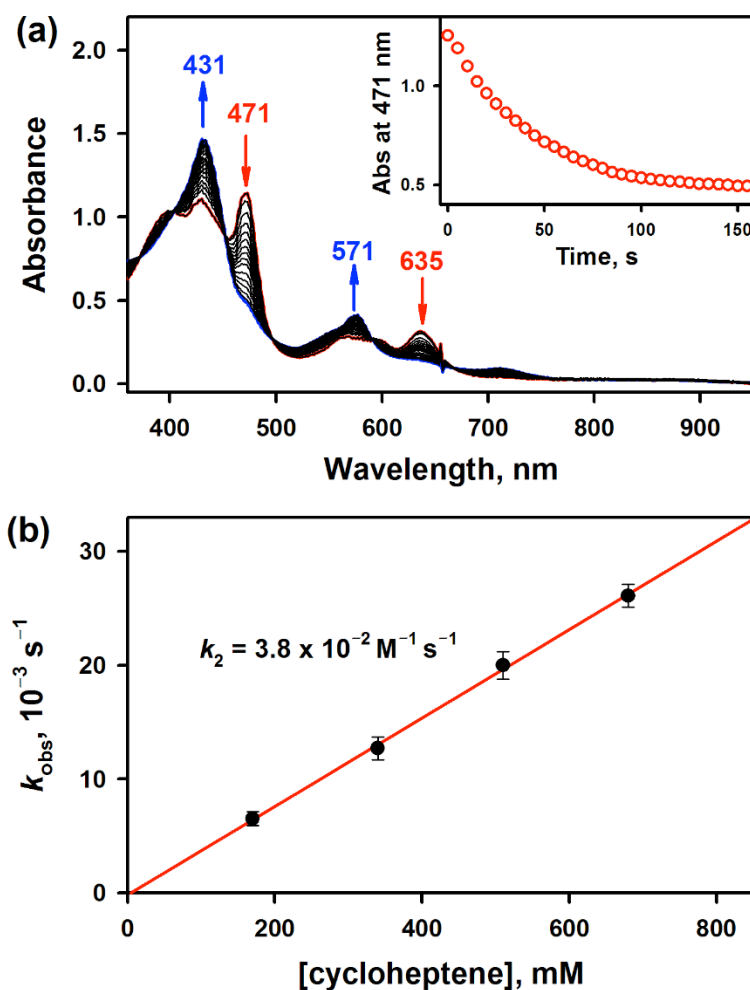


Figure S18. (a) UV-vis spectral changes observed in the formation of **2** (blue line) upon addition of cycloheptene (0.51 M) to a CH₃CN solution of [(TPFC)Mn^{III}(OH)]⁻ (**3**) (0.030 mM, red line), which was produced by adding TMAH (0.60 mM) to a CH₃CN solution of [(TPFC)Mn^{III}] (0.030 mM), under an air atmosphere at -20 °C. Inset shows the time course of absorbance monitored at 471 nm due to the decay of **3**. (b) Plot of k_{obs} against cycloheptene concentration for the formation of **2** in the O₂-activation by [(TPFC)Mn^{III}] (0.030 mM) with O₂ in the presence of TMAH (0.60 mM) under an air atmosphere in CH₃CN at -20 °C to determine the second-order rate constant, k_2 .

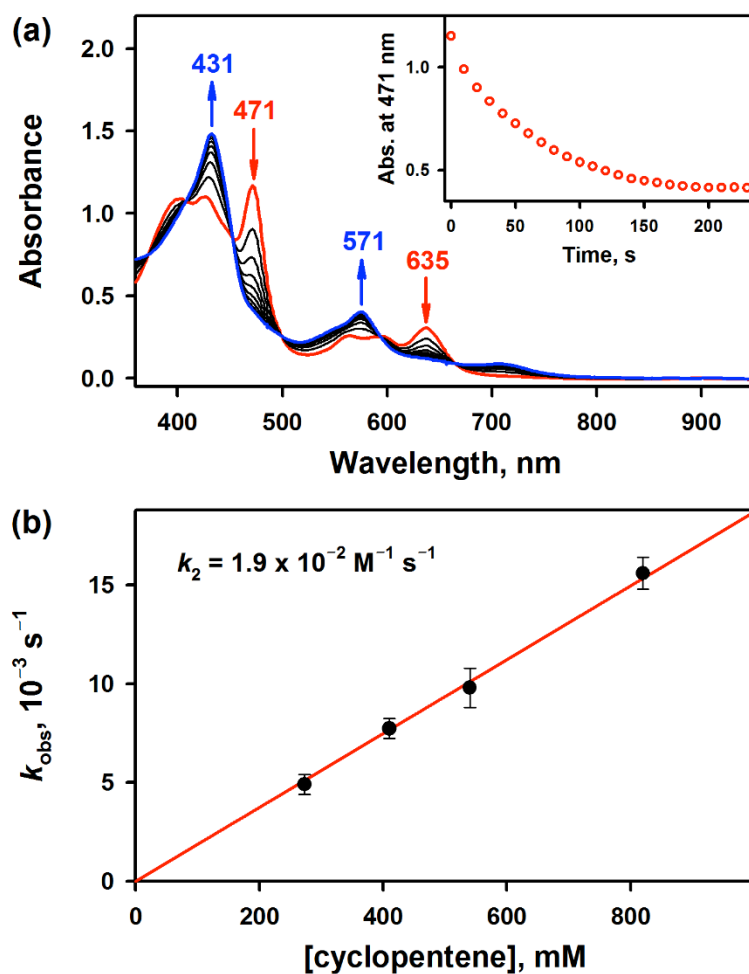


Figure S19. (a) UV-vis spectral changes observed in the formation of **2** (blue line) upon addition of cyclopentene (0.82 M) to a CH₃CN solution of [(TPFC)Mn^{III}(OH)]⁻ (**3**) (0.030 mM, red line), which was produced by adding TMAH (0.60 mM) to a CH₃CN solution of [(TPFC)Mn^{III}] (0.030 mM), under an air atmosphere at -20 °C. Inset shows the time course of absorbance monitored at 471 nm due to the decay of **3**. (b) Plot of k_{obs} against cyclopentene concentration for the formation of **2** in the O₂-activation by [(TPFC)Mn^{III}] (0.030 mM) with O₂ in the presence of TMAH (0.60 mM) under an air atmosphere in CH₃CN at -20 °C to determine the second-order rate constant, k_2 .

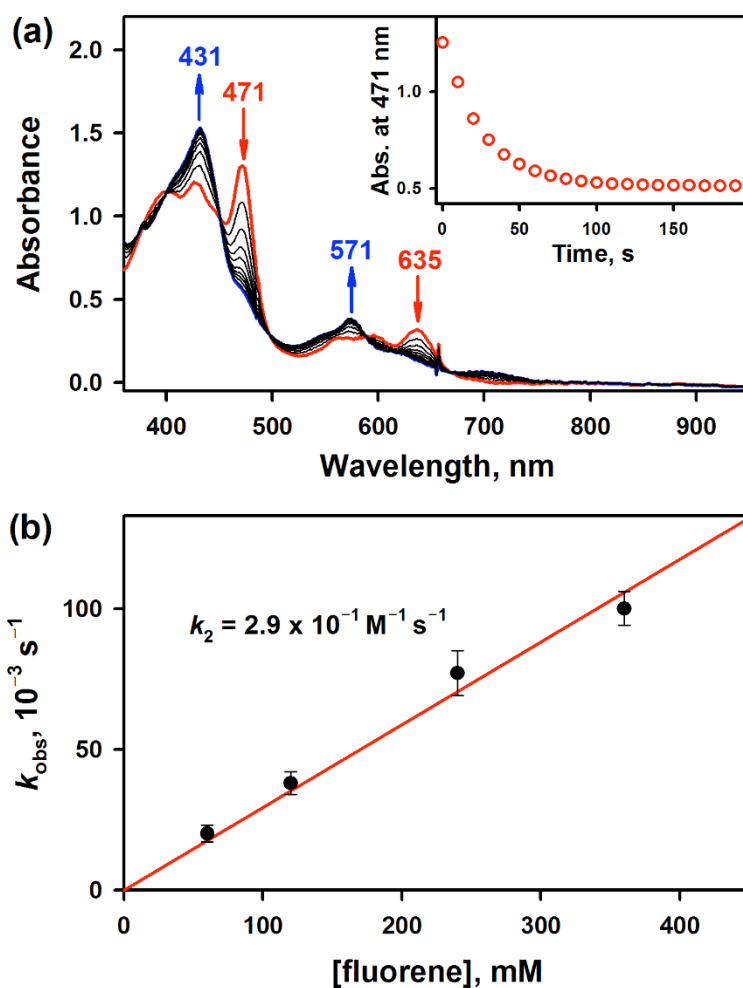


Figure S20. (a) UV-vis spectral changes observed in the formation of **2** (blue line) upon addition of fluorene (0.12 M) to a CH₃CN solution of [(TPFC)Mn^{III}(OH)]⁻ (**3**) (0.030 mM, red line), which was produced by adding TMAH (0.60 mM) to a CH₃CN solution of [(TPFC)Mn^{III}] (0.030 mM), under an air atmosphere at -20 °C. Inset shows the time course of absorbance monitored at 471 nm due to the decay of **3**. (b) Plot of k_{obs} against fluorene concentration for the formation of **2** in the O₂-activation by [(TPFC)Mn^{III}] (0.030 mM) with O₂ in the presence of TMAH (0.60 mM) under an air atmosphere in CH₃CN at -20 °C to determine the second-order rate constant, k_2 .

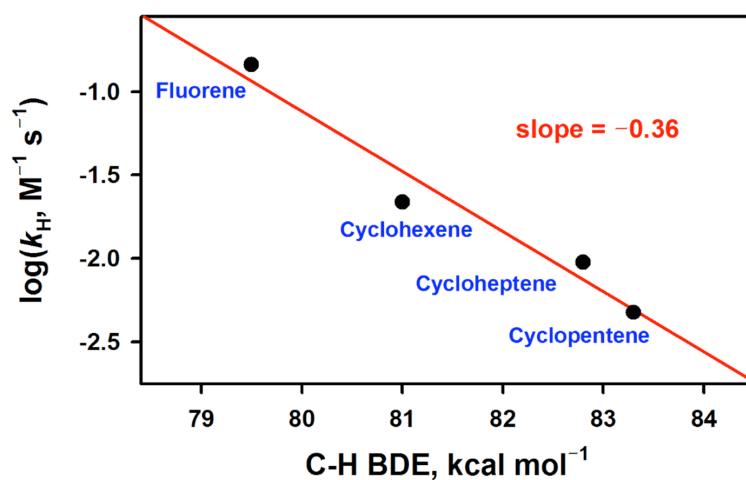


Figure S21. Plot of $\log k_H$ vs BDE of substrate. The k_H values were obtained by dividing the second-order rate constants (k_2) by the numbers of equivalent target C-H bonds in the substrates (i.e., 4 for cycloalkenes and 2 for fluorine). The slope in the linear correlation is 0.36 ± 0.04 , which corresponds to the Bell-Evans-Polanyi α value of 0.42 ± 0.05 .

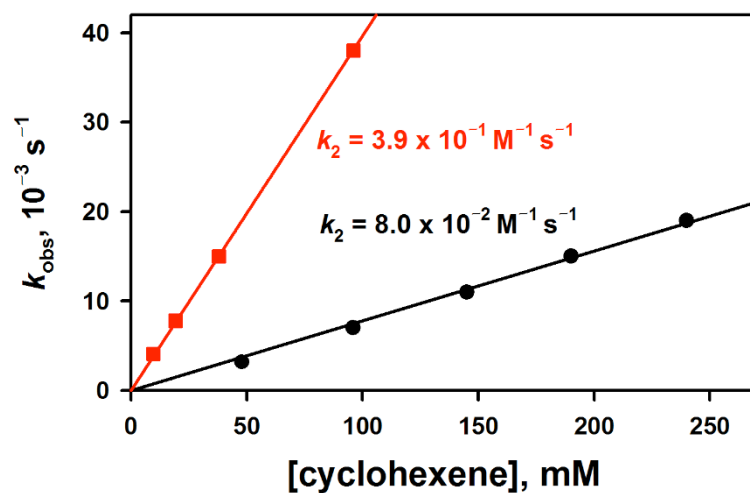


Figure S22. Plots of k_{obs} against cyclohexene concentration for the formation of **2** in the O_2 -activation by $[(\text{TPFC})\text{Mn}^{\text{III}}]$ (0.030 mM) in the presence of TMAH (0.60 mM) in air-saturated (black circles) and O_2 -saturated (red squares) CH_3CN at $-20\text{ }^\circ\text{C}$ to determine the second-order rate constants, k_2 . The formation rate constant in O_2 -saturated CH_3CN is approximately 5 times larger than that in air-saturated CH_3CN .

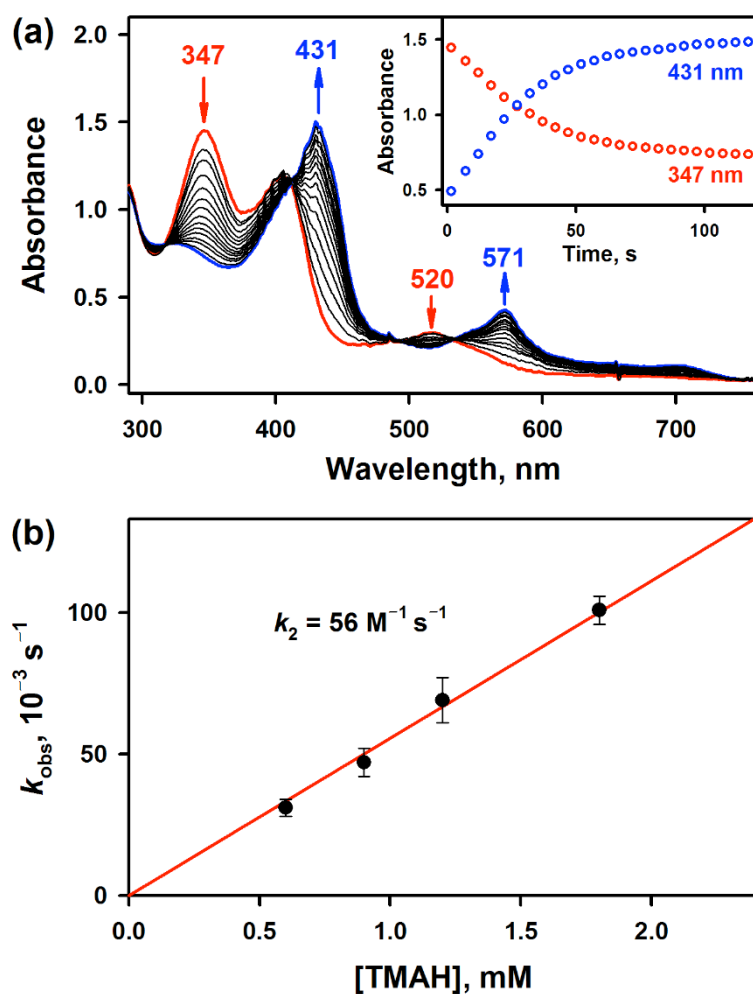


Figure S23. (a) UV-vis spectral changes observed for the conversion of **1** (0.030 mM, red line) to **2** (blue line) upon addition of TMAH (0.60 mM) to a CH₃CN solution of **1** at –40 °C. **1** was generated by adding ⁵PhIO (0.060 mM) to a CH₃CN solution of [(TPFC)Mn^{III}] (0.030 mM) at –40 °C. Inset shows the time course of absorbance monitored at 347 nm and 471 nm due to the decay of **1** and formation of **2**, respectively. (b) Plot of k_{obs} against TMAH concentration for the conversion of **1** (0.030 mM) to **2** in the presence of TMAH in CH₃CN at –40 °C to determine the second-order rate constant, k_2 .

References

- (S1) Gross, Z.; Golubkov, G.; Simkhovich, L. *Angew. Chem., Int. Ed.* **2000**, *39*, 4045.
- (S2) Bougher, C. J.; Liu, S.; Hicks, S. D.; Abu-Omar, M. M. *J. Am. Chem. Soc.* **2015**, *137*, 14481.